# SINGLE TURN EXTRACTION*

Invited Paper

M. M. Gordon
Michigan State University
East Lansing, Michigan

## Introduction and Summary

The salient features of the resonance extraction system for the MSU cyclotron have already been described in a series of studies including: the generation of turn separation via the resonance mechanism[1], the design calculations for the electrostatic and magnetic channels[2], and the development of the air-core magnetic channel[3]. A report issued in connection with this conference describes the status and presents pertinent data on the performance of the cyclotron, including the extraction system[4]. Since the issuing of that report, the electrostatic channel has been installed for preliminary tests. Experiments have verified that a suitable field bump drives the beam into this channel with clean turn separation, and that the turn pattern observed under these conditions agrees with orbit computations; the upper part of Fig. 1 shows the turn pattern obtained from the differential and integral probe with the deflector in place (the azimuth of the probe is 160° before that of the channel entrance)[5]. The air-core magnetic channel is approaching completion and when this channel is installed, the extraction system will become fully operational.

During the past year external beams have been obtained by accelerating $H^-$ ions and using electron stripping by thin foils for beam extraction. The resonance method has been applied successfully with these beams to achieve both turn separation and single-turn extraction. The lower portion of Fig. 1 shows a deuteron spectrum from the (p,d) reaction on $^{12}C$ at 45° (lab) with 31.1 MeV protons. The overall resolution of the peaks is 90 keV FWHM; concurrent precision pulser tests showed electrical noise to be 70 keV and the target thickness was 50 keV. Since the on target beam was essentially unanalyzed and since the energy gain per turn in the cyclotron was 160 keV, the observed excellent resolution must result from single-turn extraction, and clearly demonstrates the merit of such a system. (The complete experiment measured such spectra over the full range of scattering angles and required 14 hours of continuous running time; during this time there was no detectable change in proton energy, or energy resolution evidencing the remarkable stability of the cyclotron.)

The present paper deals with certain aspects of the resonance-extraction method which have not been treated before, or else only incompletely, and aims to clarify certain features of this process. The section on instantaneous centers for accelerated orbits demonstrates that an ideal central ray exists for accelerated orbits such that a beam centered on this ray will exhibit only insignificant coherent oscillations over most of the acceleration range. The section on the resonance extraction mechanism provides a semi-quantitative analysis of the orbit displacement produced by this mechanism and the influence of the field bump parameters. The section on voltage and field errors analyzes the effect of such errors and discusses the tolerances required for reliable performance. The succeeding section demonstrates that for an internal beam of 0.1 inch radial width the resonance extraction system does indeed produce clean turn separation, and discusses the factors which have brought the axial instability of the coupling resonance under control. The last, and perhaps most important, section describes the procedure for optimizing the frequency so that for single-turn extraction the energy spread of the beam is minimized; this section also provides a comparison between single and multiple turn extraction with regard to energy spread and phase width in the extracted beam.

Single-turn extraction cannot be attained unless the phase width of the beam is restricted (by using slits, for example, in the central region)[5]; however, when achieved, this process has the advantage of producing an external beam whose current is proportional to the square root of the energy spread so that the fraction of the beam which survives energy analysis is maximized. Experiments which demand hyperfine energy resolution (e.g., 5 keV) also require very limited radial and axial spot-size·divergences—such demands are best fulfilled by the single-turn extraction system. Single-turn extraction with restricted phase width also produces sharply defined beam pulses which are an essential prerequisite for neutron time-of-flight studies. Finally, the single-turn extraction process offers the only certain method of achieving 100 percent beam extraction. Multi-turn extraction does, of course, yield a larger external beam current with a larger duty factor. Here, the external beam has an energy spread equal to the energy gain per turn; however, the extra current is directly proportional to the energy spread in the beam so that after energy analysis a much smaller fraction of the beam survives. Hence, multi-turn extraction is preferable mainly for experiments where duty factor or gross current considerations outweigh energy resolution considerations in importance. Considering the interests of the nuclear experimentalists, the MSU cyclotron will operate predominantly in the single-turn extraction mode; however, for those experiments where substantial duty factor is required, the machine can with equal ease operate in the multi-turn extraction mode. The resonance extraction process works effectively in either the single or multiple-turn extraction mode.

## Instantaneous Centers for Accelerated Orbits

When the ion orbits are "centered", the beam exhibits no coherent oscillation effects; that is, the turns are evenly spaced throughout each

 Reprinted from IEEE Transactions on Nuclear Science NS-13 (4), Aug 1966 

precession cycle. The achievement of the ultimate performance, in terms of reliability and efficiency, with the resonant extraction method requires a well-centered beam, such that the coherent oscillation present over the major part of the acceleration prior to extraction is negligible in amplitude compared to the orbit displacement generated by the resonance. When this requirement is fulfilled, the behavior of the orbits during extraction will be quite insensitive to their previous history inasmuch as the resonance extraction mechanism depends predominately on the variation of $\nu_r$ with E at and beyond the resonance. As will be shown here, instantaneous centers can be defined for accelerated orbits in a three sector cyclotron despite the electric gap-crossing resonance[6].

As is customary, let $(x,p_x)$ be the radial phase space coordinates of the accelerated orbit relative to the corresponding coordinates of the ideal equilibrium orbit, so that:

$$x(E,\theta) = r(E,\theta) - r_e(E,\theta) \ ,$$
$$p_x(E,\theta) = p_r(E,\theta) - p_{re}(E,\theta) \ ; \qquad (1)$$

where $(r,p_r)$ and $(r_e,p_{re})$ are coordinates of the accelerated orbit and the E. O., respectively. A phase plot is obtained by plotting x vs. $p_x$ once per revolution at a specific $\theta$ (here, always $\theta = 0$). Between the central region and the extraction region of the cyclotron, the stability limits imposed by the $\nu_r = 3/3$ resonance are quite large, and if a small first harmonic field imperfection is present, then the E.O. is displaced from the machine center. This effect manifests itself by the appearance of a fixed-point in the phase space diagram at each energy, which is not at the origin. Assuming no gap-crossing resonance, the $(x,p_x)$ points for an accelerated orbit will circulate about the fixed-point (precessional motion) and trace out an eigen-ellipse every $(\nu_r - 1)^{-1}$ turns (precessional cycle) assuming that adiabatic conditions obtain. Under these conditions a phase-space area centered on the fixed-point will remain so centered during acceleration so that the group of orbits therefore exhibits no coherent oscillation. Under adiabatic conditions coherent oscillation of a "centered" set of orbits can develop only by acceleration through the $\nu_r = 1$ resonance, as in the extraction process.

The electric gap-crossing resonance in a three-sector cyclotron has an effect similar to a first harmonic field bump; however, since it is an acceleration effect, a displaced E.O. cannot be defined in the usual sense. Nevertheless, an instantaneous center can be defined for accelerated orbits in terms of a "quasi-fixed" point in the $(x,p_x)$ diagram. This point is determined at a given energy by requiring that its $(x,p_x)$ coordinates be the same at the beginning and end of one accelerated revolution (which reduces to the usual fixed-point definition in the limit of zero acceleration). A special routine ("Disport") has been added to the General Orbit Code ("Goblin") which computes these quasi-fixed point orbits using a process similar to that for unaccelerated closed orbits[7]. Input data for this routine consists of E.O. information and the phase $\phi$ vs. E for a given magnetic field, such data being directly available from the output of the Cyclotron Operation Program ("Set-Op")[8]. The Disport routine has been quite effective in finding the quasi-fixed points with an error of less than $10^{-5}$ inches (with only a few iterations in most cases); as expected, it fails to find such points when $\nu_r$ is very close to unity.

Figure 2 shows quasi-fixed points for two different fields as a function of energy. One field is for 25 MeV protons ($\nu_r = 1$ at E = 22.9 MeV) and the other is for 52 MeV protons ($\nu_r = 1$ at E = 47.8 MeV). Since the dee voltage is set to give the same total number of turns in both fields, the first circled point in each case (5 and 10 MeV) corresponds to the same number of turns (about 40); moreover, the interval between successive circled points represents about 20 turns. As can be seen, the shape of the curves in Fig. 2 is very similar for both fields; furthermore, the evolution of these curves is closely correlated with the number of turns. This result is not surprising since the strength of the gap-crossing resonance varies inversely with the number of turns to the given E. The variation of the quasi-fixed points with E depends on the phase $\phi(E)$; the change in these points for different initial phases will be small if $\phi(E)$ remains close to zero or if the difference in initial phase is small.

Tests have shown that the quasi-fixed points do indeed define instantaneous centers for accelerated orbits. For example, starting from the quasi-fixed point at 10 MeV in the 25 MeV proton field, an orbit was accelerated forward to the extraction region and also backward to the central region. Figure 3 shows plots of $\Delta x$ vs. $\Delta p_x$ derived from these computations, where $(\Delta x,\Delta p_x)$ is the coordinate displacements of the accelerated orbit from the quasi-fixed point at the same E. In both the forward and backward acceleration cases, the plots show a slow spiraling outward of successive points. What is truly remarkable is that over the energy range from 2.8 MeV to 22.0 MeV (165 turns out of a 215 total for the complete acceleration) the magnitude of the displacement does not exceed 0.02 inches. Clearly then, a phase-space area associated with this accelerated orbit will have a completely negligible amount of coherent oscillation over this energy range. Indeed, these results are also in close accord with experimental observations reported elsewhere at this conference[4,5].

## Resonance Extraction Mechanism

The extraction studies to be described here were carried out with the 52 MeV proton field since this field most closely resembles that used in our previously reported work[1]. With 66.26 kV dee to ground, the peak energy gain per turn is $E_1 = 247$ keV; the final energy for this field was designed to be 51.97 MeV ($\nu_r = 0.8$), at which the phase $\phi = 32.3^0$ for the central ray. The first harmonic field bump used here corresponds to that produced by the harmonic coils of the cyclotron; namely,

$$b(r,\theta) = b_1(r)\cos(\theta-\theta_o) \ , \qquad (2)$$

where $b_1(r)$ has a flat maximum in the vicinity of r = 27 inches ($\nu_r = 1$) and the magnitude at this point can be varied up to 10 gauss (200 amps); in addition, the azimuthal location $\theta_o$ and the magnitude of $b_1$ can be independently varied.

Using a field bump with 2 gauss amplitude and $\theta_o = 0$, and starting on the quasi-fixed point at 15 MeV, the orbit was accelerated to the extraction radius. The phase plot for the end of this orbit is shown in Fig. 4 with points circled from turn $\tau = 192$ to 218 (turns are numbered from the center of the machine). The $\nu_r = 1$ resonance occurs at $\tau = 202$. The small "hook" preceding the circled points covers about 40 turns and demonstrates how well centered this orbit is prior to the resonance region (the diameter of the hook is 0.015 inches). This plot shows clearly the resonance extraction mechanism: as the orbit accelerates through the resonance ($\tau = 192$ to 208) there is a steady growth in its displacement up to 0.25 inches; as $\nu_r$ continues to fall even more rapidly below unity, this displacement is converted to an oscillation amplitude and the orbit then precesses with rapidly increasing angular speed. With a proper choice of $\theta_o$ this precessional motion will reinforce radius gain per turn and thereby yield an exceptionally large $\Delta r$ at the position of the channel septum. In this way the resonance extraction mechanism generates turn separation in the beam.

An analytical treatment of the resonance transition using the WKB approximation (neglecting non-linear effects) yields the following result for the displacement generated:

$$A = \pi R(b_1/B_o)(\Delta\tau) \ ; \qquad (3)$$

where

$$(\Delta\tau)^{-2} = \left|\frac{d\nu_r}{dE}\right| E_1\cos\phi \ ; \qquad (4)$$

R is the mean orbit radius at $\nu_r = 1$, $b_1$ and the average field $B_o$ are evaluated at R, and $E_1\cos\phi$ is the energy gain per turn at $\nu_r = 1$. The quantity $(\Delta\tau)$ represents the "effective duration" of the resonance; i.e., the orbit displacement takes place effectively during $\Delta\tau$ turns bracketing the resonance. According to this analysis, the orbit center is displaced in a direction $\theta_c$ relative to the machine center, where:

$$\theta_c = \theta_o - 90^o \ . \qquad (5)$$

These formulae are obtained by assuming $\nu_r$ varies linearly with E about $\nu_r = 1$; however, this is not the case for actual fields so that these formulae can yield only approximate results. For the field under consideration here $|d\nu_r/dE| = 0.02$/MeV; taking $E_1\cos\phi = 0.25$ MeV, Eq. (4) yields $(\Delta\tau) = 14$ turns. The orbit whose phase plot is depicted in Fig. 4 passes $\nu_r = 1$ on $\tau = 202$, and $(\Delta\tau) = 14$ implies that the resonant displacement occurs between $\tau = 195$ and 209, which is in fair agreement with the observed result. For $b_1 = 2$ gauss Eq. (3) then yields A = 0.18 inches whereas the results shown in Fig. 4 indicate A = 0.25 inches. For $\theta_o = 0$, Eq. (5) yields $\theta_c = -90^o$; that is, for a phase plot at $\theta = 0$ the points should displace in the negative $p_x$ direction; Fig. 4 agrees reasonably well with this conclusion.

A set of orbits was calculated using the same initial conditions as above (cf. Fig. 4) with bump strengths of 0, 2, and 4 gauss, and with $\theta_o$ varying in 45° steps. The resultant array of $(x,p_x)$ points for these 17 orbits is shown in Fig. 5 at $\tau = 216$. This figure demonstrates that the amount of orbit displacement is proportional to the bump strength and that the direction of the displacement is directly correlated with $\theta_o$.

The septum of the electrostatic deflector is located near r = 29 inches at $\theta = -21^o$ (on the down side of a hill). Examination of the orbits obtained with a 2 gauss bump shows: for $\theta_o = 0$, extraction occurs at $\tau = 219$ with $\Delta r = 0.36$ inches; for $\theta_o = 45^o$, extraction also occurs at $\tau = 219$, but with $\Delta r = 0.29$ inches; for $\theta_o = -45^o$, extraction occurs at $\tau = 220$, with $\Delta r = 0.38$ inches. All other $\theta_o$ values must be rejected since acceptable $\Delta r$ values occur either too early or too late. The fact that $\theta_o = -45^o$ yields extraction one turn after the $\theta_o = 0, 45^o$ cases is consistent with the amount of precession occuring during the extra turn. Thus, the optimum $\theta_o$ value for the field bump depends quite strongly on the number of turns between the resonance and channel entry. After checking $\theta_o = 15^o$ and $-15^o$, the value $\theta_o = 0$ was selected as the best value here for the 2 gauss bump; the final E (= 51.82 MeV) and $\phi$ (= 30.0°) agree closely with the design values for this field. The remainder of the computations described here were made with this bump choice.

## Voltage and Field Errors

If the dee voltage is varied by $\delta V_o$, the number of turns $\tau$ varies by:

$$-\delta\tau = \tau(\delta V_o)/V_o \ . \qquad (6)$$

The orbit corresponding to Fig. 4 was recalculated for 12 different $V_o$ values in steps of $(\delta V_o)/V_o = \pm 1.1 \times 10^{-3}$ (for which $\delta\tau$ varies by about 0.25). All of these orbits arrive in the vicinity of r = 29 inches at $\theta = -21^o$ with $\Delta r$ values between 0.33 and 0.38 inches, and with final $\tau$ from 218 to 221. Figure 6 displays the final E values plotted against the final r values (assuming r > 29 inches). The final $\phi$ values range from 30° to 34° and are directly correlated with the E values. As shown in Fig. 6, for a fixed r value the energy varies by only 6 keV for a variation of $\delta\tau = \pm 1$. These results clearly indicate that small voltage variations can be used to precisely adjust the beam position in the channel, and that one turn more or less out of 220 is not significant (a consequence of orbit centering). These results also show that $(\delta V_o)/V_o = \pm 1.1 \times 10^{-3}$ produces an energy

 

variation of 60 keV in the extracted beam. Consequently, once the voltage has been set, its regulation must be strict.

For a uniform fractional field variation $(\delta B/B)$, the value of $\tau$ varies by:

$$\delta\tau = \frac{\delta B}{B}\,\frac{2\pi}{E_1^2}\int\frac{E\sin\phi\,dE}{(\cos\phi)^3}$$

$$\approx 2\pi(\delta B/B)\tau^2\,\bar{\phi}_f\ , \qquad (7)$$

where $\bar{\phi}_f$ is an average of $\phi$ near the end of acceleration. Thus, the field error tolerance varies as $\tau^{-2}$. The foregoing result was derived for a frequency error which is at least approximately equivalent to a field error. Using the same reference orbit (Fig. 4), but starting at E = 0.117 MeV, the frequency was varied in steps of $\pm 10^{-5}$ and the calculation repeated. The results show that $(\delta B/B) = \pm 10^{-5}$ yields $\delta\tau = \pm 0.25$, which agrees approximately with the predictions of Eq. (7). Thus, an error $(\delta B/B) = 10^{-5}$ is equivalent to an error $(\delta V_o/V_o) = 10^{-3}$.

## Turn Separation and Axial Stability

A set of orbits was computed whose initial $(x,p_x)$ coordinates lie on an eigen-ellipse about the 15 MeV quasi-fixed point. The size of the ellipse was chosen so that the radial width of the set of orbits at 15 MeV was 0.1 inches, since this value is consistent with the measurements made with the differential probe on the actual cyclotron beam[5]. The dee voltage for this computation was decreased $2.2 \times 10^{-3}$ so that the central ray corresponds to the center point on the line in Fig. 6 for $\tau = 220$; this adjustment improves the positioning of the phase-space area relative to a septum at r = 29 inches and also gives E = 51.917 MeV and $\phi = 32.2^\circ$ in closer agreement with the design values. Starting from 15 MeV these orbits were accelerated for 158 turns to $\tau = 220$, where they "enter" the electrostatic channel.

Figure 7 shows the evolution of the radial phase space area from $\tau = 204$ to 220. The picture starts one turn after $\nu_r = 1$, and from $\tau = 204$ to 209 the orbit displacement effect predominates; thereafter, the precession of the displaced orbits takes hold and increases in speed on succeeding turns. Between $\tau = 204$ and 209 the increase in radius per turn is mainly the acceleration effect, whereas the decrease in $p_r$ is mainly orbit displacement (see Fig. 4). The turn separation between $\tau = 219$ and 220 equals 0.27 inches which is more than adequate since a 50 keV energy spread in the beam increases the turn width by only 0.1 inches.

These orbits all start with the same $\phi$ values at E = 15 MeV; however, at $\tau = 220$ the variation in energy is 17 keV and the phase spread is 1.7°; moreover, these E and $\phi$ variations are not correlated with each other nor with the radial position. This incoherence results from the radial oscillations of these orbits about the central ray during the 158 turns of acceleration. This effect would be somewhat larger if the orbits had been accelerated from the center for the full 220 turns.

Axial instability at the $\nu_r = 2\nu_z$ coupling resonance has turned out less troublesome than originally anticipated[1]. The results of magnetic field measurements have shown that the intrinsic first harmonic of the cyclotron magnet in the neighborhood of the resonance is about one gauss; in addition, the individual Fourier coefficients are known. The field produced by the harmonic coils, Eq. (2), can be set with an accuracy of ± 0.05 gauss (at $\nu_r = 1$) and the azimuth $\theta_o$ can be varied in steps of 3°. Hence, it is not difficult to produce and maintain a field bump with 1 to 2 gauss amplitude near the resonance with quite adequate accuracy, such that turn separation can be produced while maintaining satisfactory axial stability. The danger of the coupling resonance is further mitigated by the fact that the dee aperture is 1.5 inches, whereas the axial width of the beam desired by the nuclear experimentalists is only 0.4 inches. Since the axial growth, when it occurs, lasts only a few turns, the extra space provided by the dee aperture easily avoids any beam loss.

For the set of orbits depicted in Fig. 7 the coupling resonance causes the axial amplitude to double; however, the amplitude thereafter decreases to its original size before the orbits arrive at the channel septum. Since more than enough turn separation was produced by the 2 gauss bump, the strength of this bump could be reduced such that adequate turn separation would be obtained without any significant axial growth.

## Frequency Optimization and Energy Resolution

To an observer traveling with an rf pulse there is some position along the pulse at which the ion density has its maximum—this point of maximum density defines the "central phase". When this rf pulse is extracted, if the energy spread in the neighborhood of the central phase has been minimized, then ideal conditions will obtain; for in this situation the amount of beam current surviving energy analysis will be maximized. Because of the central hump in the field and because the ions are accelerated into the non-isochronous edge region before extraction, the central phase will vary with energy; in addition, this phase must initially have a positive value (i.e., lagging the rf voltage) in order to survive the strong electric defocusing on the first turns. If the field is reasonably isochronous then the rf frequency can always be adjusted such that at extraction the energy variation at the central phase is minimized.

The phase slip per turn is given by:

$$d\phi/d\tau = \omega_{rf}T(E) - 2\pi h\ , \qquad (8)$$

where $\omega_{rf}$ is the rf angular frequency, h is the harmonic ratio, and T(E) is the rotation period of the ion at the energy E. Zero phase is defined by

specifying that the energy gain per turn is given by:

$$dE/d\tau = E_1 \cos\phi \,, \qquad (9)$$

where $E_1$ is the peak value. Let $\phi_o$ be the initial value of the central phase at E = 0 (actually, $\phi_o$ must be obtained by extrapolation of $\phi(E)$ since these equations do not apply for $E \to 0$), and suppose that the central phase is extracted on turn $\tau_f$ with energy $E_f$. The energy spread between all the ions extracted on turn $\tau_f$ will be minimized at the central phase provided:

$$E_f(\phi_o \pm \Delta\phi_o) = E_f - 1/2(\Delta\phi_o)^2 E'' \,, \qquad (10)$$

that is, provided the ions at the central phase have the maximum energy. This condition can be satisfied by adjusting the frequency such that:

$$\int \frac{\sin\phi \, dE}{(\cos\phi)^3} = 0 \,, \qquad (11)$$

where $\phi(E)$ is the central phase and the integration extends from E = 0 to $E_f$; in this case E" becomes:

$$E'' = \cos^2\phi_o \cos\phi_f \int \frac{(1 + 2\sin^2\phi)\, dE}{(\cos\phi)^5} \,, \qquad (12)$$

where $\phi_f = \phi(E_f)$ is the final value of the central phase. Furthermore, since $\Delta(\sin\phi_o) = \Delta(\sin\phi_f)$, the same relations hold with $\phi_f$ and $\Delta\phi_f$ replacing $\phi_o$ and $\Delta\phi_o$. The condition, Eq. (11), not only maximizes the energy of the central phase on the final turn $\tau_f$, but in addition, it also minimizes the number of turns to reach the final energy $E_f$ at this phase value (thereby optimizing the acceleration efficiency).

As a simple example, consider a field which is perfectly isochronous relative to the frequency $\omega_{rf}$. Then the condition, Eq. (11), requires that the frequency be lowered by an amount $\delta\omega_{rf}$ given by:

$$\frac{\delta\omega_{rf}}{\omega_{rf}} = \frac{E_1 \sin\phi_o}{\pi h E_f} \,; \qquad (13)$$

in this case, $\phi_f = -\phi_o$, and E" = $E_f$ so that:

$$E_f(\phi_o \pm \Delta\phi_o) = E_f[1 - 1/2(\Delta\phi_o)^2] \,, \qquad (14)$$

and,

$$E_f = \tau_f E_1 (\sin\phi_o)/\phi_o \,. \qquad (15)$$

For a non-isochronous field if $\phi(E)$ remains small in magnitude then the condition, Eq. (11), is approximately equivalent to requiring that the average of $\phi(E)$ be 0; under these same conditions, E" = $E_f$, the isochronous field value. Thus the spread in final energies $\Delta E_f$ corresponding to an initial phase range from $\phi_o - \Delta\phi_o$ to $\phi_o + \Delta\phi_o$ is given by:

$$\frac{\Delta E_f}{E_f} \simeq \frac{1}{8}(2\Delta\phi_o)^2 \,, \qquad (16)$$

where $2\Delta\phi_o$ is the total spread in the initial phases. This result is obtained from frequency optimization even though the field is not isochronous and even for $\phi_o \neq 0$.

After synthesizing a magnetic field the "Set-Op" program sets the final energy $E_f$ at the point where $\nu_r = 0.8$ and sets the dee voltage so that $E_1 = E_f/210$; it then finds the rf frequency for which the condition, Eq. (11), is satisfied by direct numerical integration[8]. The initial value for the central phase has tentatively been set at $\phi_o = +30^\circ$ in all cases for first harmonic acceleration. Figure 8 shows plots of $\phi$ vs. E for the 25 MeV and 52 MeV proton fields as obtained from the "Set-Op" program. As can be seen, the field hump at the center of the machine causes the phase to drop sharply from its initial value; this phenomenon has the favorable effect of shifting the phase from an initially good electric focusing value toward the optimum acceleration value. In the 25 MeV proton case the linear fall-off of $\phi$(E) shows that the field is quite isochronous over most of the energy range; the subsequent rise at the end results from the non-isochronous edge region of the field; the final energy here is 25.56 MeV at which $\phi_f = +1.4^\circ$. For the 52 MeV proton case the field deviates from isochronism over most of the energy range in order to improve the axial focusing in the region from 40 to 45 MeV; here $E_f$ = 51.97 MeV with $\phi_f = 32.3^\circ$ and E" = 1.23 $E_f$. The extraction studies described above (and below) are based on the $\phi$ vs. E curves shown in Fig. 7.

Starting from its centered position at 15 MeV, the orbit depicted in Fig. 4 was decelerated for 62 turns where it reached the energy E = 0.117 MeV at which the phase $\phi = 21.5^\circ$. Starting at E = 0.117 MeV a set of orbits was computed with initial $\phi$ values varying from the central phase by $\Delta\phi_o = \pm 1.5^\circ, \pm 3^\circ, \pm 4^\circ, \ldots, \pm 9^\circ$ and with initial $(r, p_r)$ all equal to the central phase value (this is justified since the phase range considered is small). These orbits were computed out to the point where they "enter" the electrostatic channel and the resultant final values of r and E as a function of $\Delta\phi_o$ are shown in Fig. 9. For the central phase ($\Delta\phi_o \cong 0$), r = 29.011 for $\tau$ = 219 and r = 28.655 for $\tau$ = 218; consequently, the "septum" was assumed to be at r = 28.655, and orbits arriving at the septum position ($\theta = -21^\circ$) with r less than this value on one turn and then with r greater than this value on the next turn were assumed to "enter" the electrostatic channel. Thus, orbits with $\Delta\phi_o$ between - 4.25 and + 5.85 enter on turn $\tau$ = 219, while those with values between - 4.25 and - 6.10 or between 5.85 and 7.95 enter on $\tau$ = 220; only those orbits which arrive on turns 219 and 220 are shown—those with larger $|\Delta\phi_o|$ arrive on later turns. It is important to note that for all these orbits the final radius gain per turn $\Delta r$ = 0.30 to 0.38 inches; this achievement of good turn separation for all these

 

orbits results from their being relatively well centered prior to extraction (at 40 MeV the $(x,p_x)$ values varied by only 0.03 inches).

The curves shown in Fig. 9 for E vs. $\Delta\phi_o$ are very similar to those shown for r vs. $\Delta\phi_o$. The parabolic shape of the E vs. $\Delta\phi_o$ curve for $\tau = 219$ indicates that the frequency was chosen quite close to the correct value for giving the central phase the maximum energy on this turn (actually, the maximum occurs at about + 0.4°). The "side-bands" shown for $\tau = 220$ are each about 2° wide; the side-bands for succeeding turns become progressively narrower—the starting point for successive side-bands is given approximately by:

$$(\Delta\phi_o)^2 = 2|\Delta\tau|/\tau\,, \qquad (17)$$

where $\Delta\tau$ is an integer.

The location of the "septum" at r = 28.655 gives the maximum possible phase width to the "parabola" on turn 219 in Fig. 9, viz., 10.1°; these results clearly demonstrate that single turn extraction is not possible unless the phase width $\Delta\phi_o$ is less than this value. If the r value for the septum were increased the $\tau = 219$ parabola would shrink and the $\tau = 220$ side-bands would expand and move inward, so that when the septum line reached r = 29.011, $\tau = 220$ would occupy the central parabola (for this dee voltage, however, the turn separation is not as good at this point). It should be kept in mind that the radial and axial phase space associated with these central rays will smear out the E vs. $\Delta\phi_o$ curves; in addition, of course, not all orbits will miss hitting a real septum.

Figure 10 shows the final phase $\phi_f$ of the orbits as they "enter" the deflector. For a given final energy $\Delta\sin\phi_f = \Delta\sin\phi_o$, independent of $\tau$; however, since the field is dropping rapidly at this radius the value of $\phi_f$ for a given $\tau$ increases rapidly with final energy, which accounts for the skewed shape of the curves in Fig. 10. The asymmetry in the two side-bands for $\tau = 220$ in Fig. 9 is explained by the fact that for negative $\Delta\phi_o$ values, the orbits have smaller $\phi_f$ and therefore gain more energy and end up with a larger r value.

The shaded area of the E vs. $\Delta\phi_o$ curve in Fig. 9 indicates the portion of these curves intercepted by an energy slice 50 keV wide across the peak of the 219 parabola; this slice covers a phase spread of 4.8° in the central parabola and only 0.5° in the $\tau = 220$ left side-band. Only one of the $\tau = 220$ side-bands is cut by this slice; however, if the septum line were increased in radius, both side-bands, and indeed many other side-bands, would also lie within this slice. Clearly, if the 50 keV slice were taken at an energy much below the peak of the $\tau = 219$ parabola, then the phase width intercepted by this slice would be considerably smaller.

As noted before, the central phase corresponds to the portion of the rf pulse with the maximum current density so that the current density decreases with increasing $|\Delta\phi_o|$. Assuming for simplicity that the current density is independent of $\Delta\phi_o$, then a small energy slice of width $\Delta E$ at the peak of the $\tau = 219$ parabola will yield a current which is proportional to the $\sqrt{\Delta E}$. However, in the side-bands, E vs. $\Delta\phi_o$ is nearly linear so that the same slice taken in the side-bands will yield a current directly proportional to $\Delta E$. Thus, if the beam is sent through a high resolution analyzer such that the resultant $\Delta E$ is very small (say 5 keV), then the proportion of beam in the vicinity of the central phase will be much larger than that contained in all the side-bands; conversely, the fraction of the beam which is discarded by the analyzer will be much smaller for those ions near the central phase than for the beam contained in the side-bands. If the frequency is not optimized so that all the beam is extracted in the side-bands (either left or right) then high resolution analysis will reject most of the ions and the surviving beam will indeed be small.

Acknowledgement

The author wishes to express his indebtedness to H. G. Blosser for many helpful suggestions and discussions, and to D. A. Johnson for assistance with the computer work.

References

1. M. M. Gordon and H. G. Blosser, "Orbit Calculations on the Extraction System for the MSU Cyclotron," Proc. of the CERN Cyclotron Conference, 236 (April, 1963).

2. J. W. Beal, "Studies of Beam Deflection for a Three-Sector Cyclotron," MSUCP-21 (Aug., 1964).

3. R. E. Berg and H. G. Blosser, "The Focusing Air-Core Magnetic Channel for the MSU Cyclotron," Particle Accelerator Conference, (Washington, Mar., 1965), 392.

4. H. G. Blosser and A. I. Galonsky, "MSU 55 MeV Cyclotron: Progress and Status," Feb., 1966 (paper at this conference).

5. H. G. Blosser, "Problems and Performance in the Cyclotron Central Region," (paper at this conference).

6. M. M. Gordon, Nucl. Instr. & Methods, 18, 19, 268 (1962).

7. M. M. Gordon, T. I. Arnette, and W. P. Johnson, Bull. Am. Phys. Soc., (April, 1964).

8. R. E. Berg, H. G. Blosser and M. M. Gordon, "Control of the MSU Cyclotron," (paper at this conference).

*Work supported by National Science Foundation.

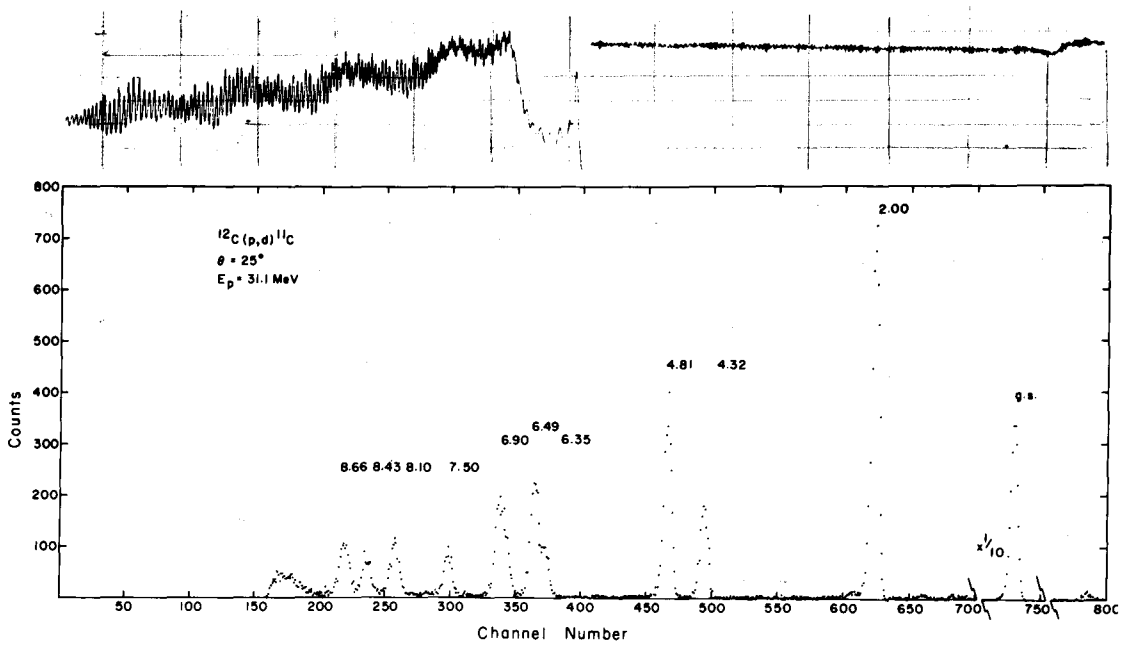


Fig. 1. Top: differential (left) and integral (right) current probe tracings demonstrating beam behavior during resonance extraction; azimuth of probe of 160° before that of electrostatic channel aperture. Bottom: deutron spectrum from $^{12}C(p,d)$ at 45° (lab) for 31.1 MeV protons showing overall resolution of 90 keV.

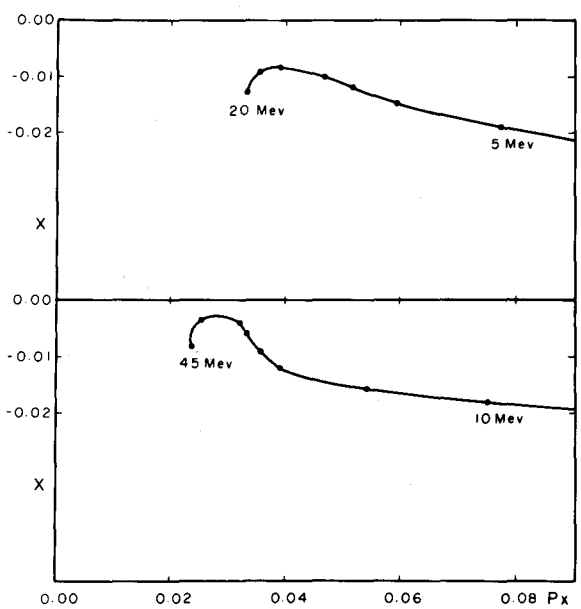


Fig. 2. Quasi-fixed points produced by electric gap-crossing resonance at $\theta = 0$ as a function of energy for 25 MeV (top) and 52 MeV (bottom) proton fields; x and $p_x$ in inches. ["$p_x$" = $(p_x)$ /qB(0)]

 

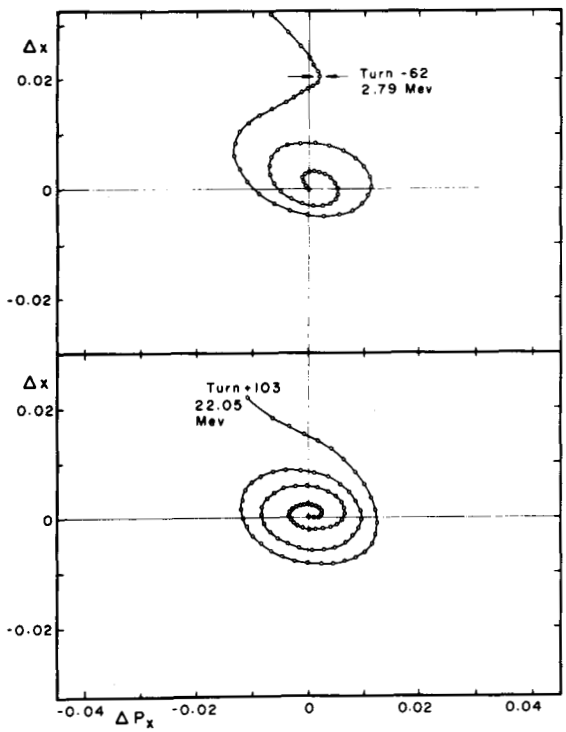


Fig. 3. Phase plots relative to quasi-fixed points in 25 MeV proton field (cf. Fig. 2) for accelerated orbits starting at 10 MeV; at top, orbit decelerated to center; at bottom, orbit accelerated to 22 MeV.

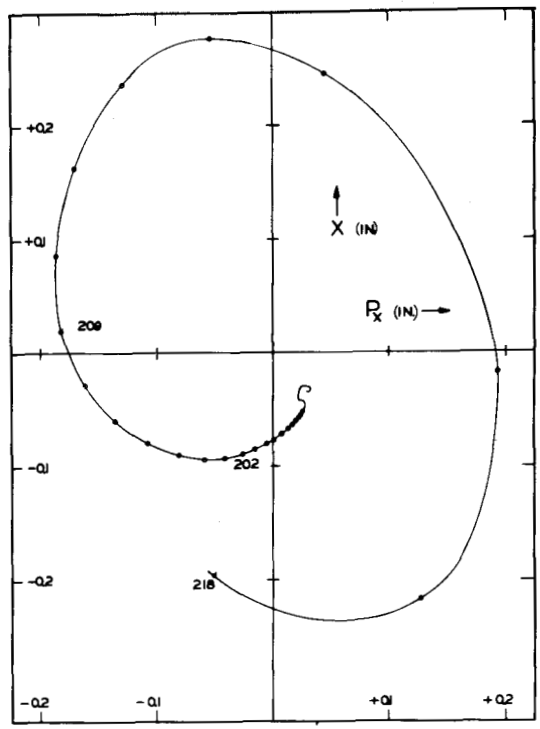


Fig. 4. Phase plot for orbit in 52 MeV proton field with 2 gauss bump at $\theta_0 = 0$, showing effect of resonance from turn 192 to 218. ["$p_x$" = $(p_x)/qB$ (0)]

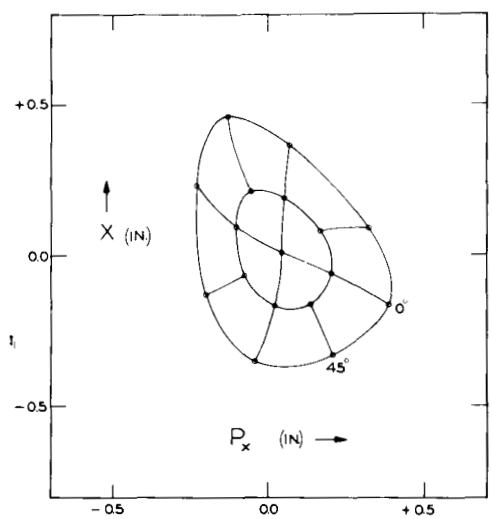


Fig. 5. Magnitude and direction of resonance displacement on turn 216 for 0, 2, and 4 gauss bump with varying azimuths ($\Delta\theta_0 = 45°$); cf. Fig. 4.

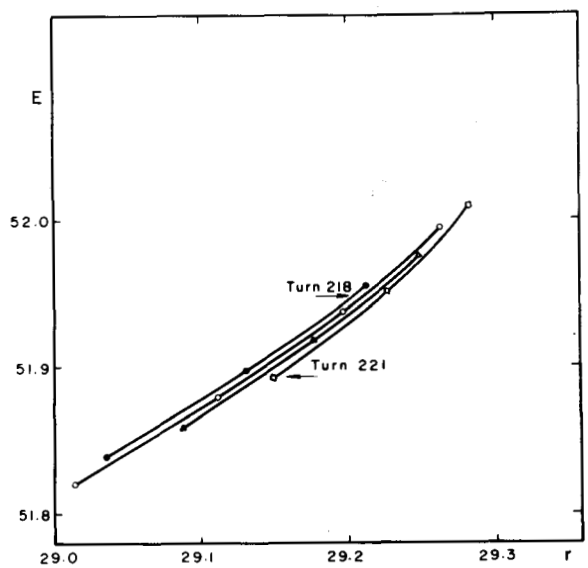


Fig. 6. Final energy (MeV) vs. final radius (inches) for orbit depicted in Fig. 4 with dee voltage varied in $\pm 1.1 \times 10^{-3}$ steps.

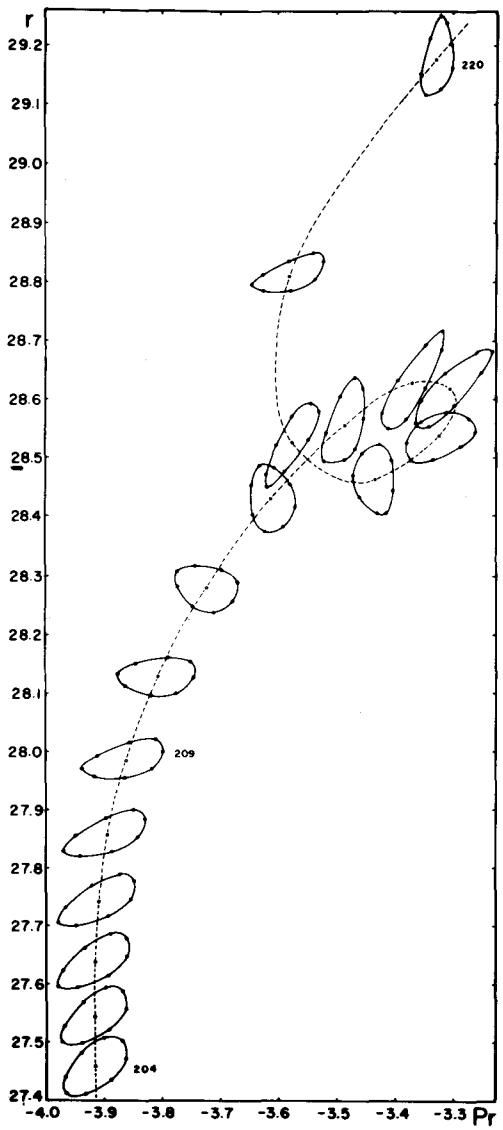


Fig. 7. Radial phase space turn pattern (at $\theta$ = - 21°) during resonance extraction (turn 204 to 220); "septum" is located at r = 29 inches ["$p_r$" = $(p_r)/qB_{(0)}$]

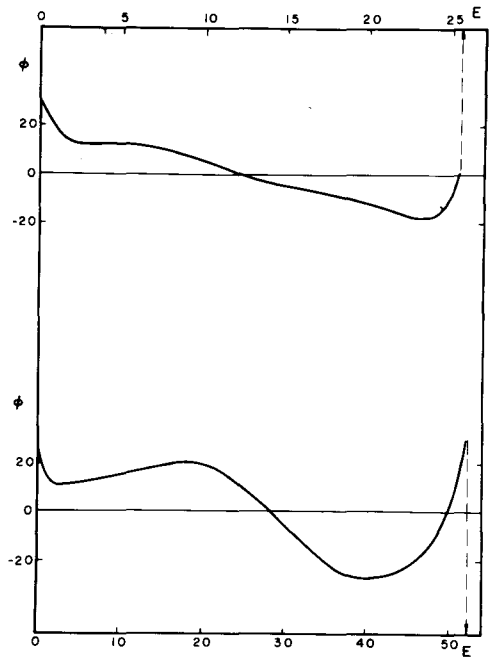


Fig. 8. Central phase $\phi$ (deg.) vs. energy E (MeV) for 25 MeV (top) and 52 MeV (bottom) proton fields.

 

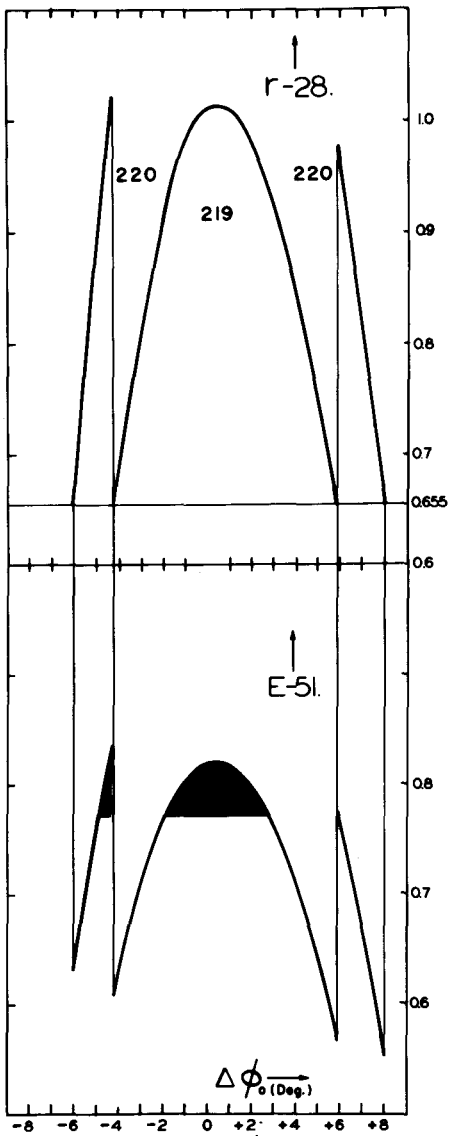


Fig. 9. Final radius r (in.) and energy E (MeV) for orbits "entering" channel on turn 219 and 220 versus initial phase $\Delta\phi_o$ (deg.); "septum" located at r = 28.655; $\Delta\phi_o$ = 0 for $\phi_o$ = 30°.

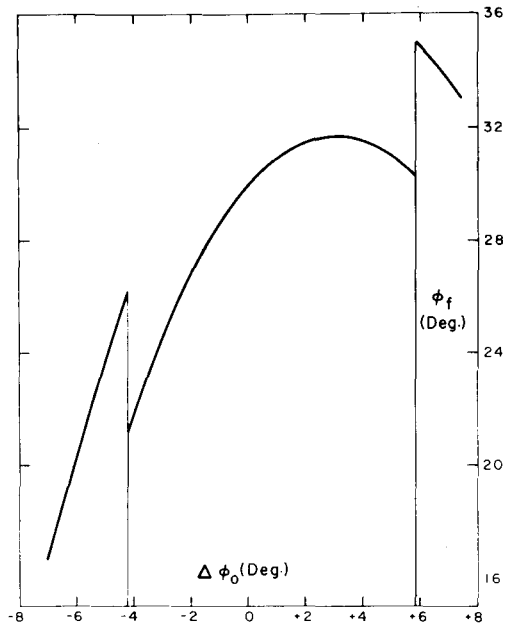


Fig. 10. Final phase $\phi_f$ vs. $\Delta\phi_o$ for orbits described in Fig. 9.